frontiers | Frontiers in Soft Matter

TYPE Original Research
PUBLISHED 20 February 2023
DOI 10.3389/frsfm.2023.1143958

OPEN ACCESS

EDITED BY
Lou Kondic,
New Jersey Institute of Technology,
United States

REVIEWED BY
Yaoyao Chen,
E Ink Company, United States
Qihui Fan,
Beijing National Laboratory for
Condensed Matter Physics (CAS), China

*CORRESPONDENCE
Raffaele Mezzenga,
raffaele.mezzenga@hest.ethz.ch

†These authors have contributed equally to this work.

SPECIALTY SECTION
This article was submitted to Granular Matter, a section of the journal Frontiers in Soft Matter

RECEIVED 13 January 2023
ACCEPTED 07 February 2023
PUBLISHED 20 February 2023

CITATION
Armanious A, Wang H, Alpert PA, Medaglia C, Peydayesh M, Zwygart AC-A, Gübeli C, Handschin S, Bolisetty S, Ammann M, Tapparel C, Stellacci F and Mezzenga R (2023), Trapping virus-loaded aerosols using granular material composed of protein nanofibrils and iron oxyhydroxides nanoparticles. *Front. Soft. Matter* 3:1143958. doi: 10.3389/frsfm.2023.1143958

Trapping virus-loaded aerosols using granular material composed of protein nanofibrils and iron oxyhydroxides nanoparticles

Antonius Armanious[1], Heyun Wang[2†], Peter A. Alpert[3†], Chiara Medaglia[4], Mohammad Peydayesh[1], Arnaud Charles-Antoine Zwygart[4], Christian Gübeli[1], Stephan Handschin[1], Sreenath Bolisetty[5], Markus Ammann[3], Caroline Tapparel[4], Francesco Stellacci[2,6,7] and Raffaele Mezzenga[1,8]*

[1]Department of Health Sciences and Technology, ETH Zurich, Zurich, Switzerland, [2]Institute of Materials, École Polytechnique Fédérale de Lausanne (EPFL), Lausanne, Switzerland, [3]Laboratory of Environmental Chemistry, Paul Scherrer Institute, Villigen, Switzerland, [4]Department of Microbiology and Molecular Medicine, University of Geneva, Geneva, Switzerland, [5]BluAct Technologies GmbH, Zurich, Switzerland, [6]Department of Bioengineering, École Polytechnique Fédérale de Lausanne (EPFL), Lausanne, Switzerland, [7]Global Health Institute, École Polytechnique Fédérale de Lausanne (EPFL), Lausanne, Switzerland, [8]Department of Materials, ETH Zurich, Zurich, Switzerland

The ongoing COVID-19 pandemic has revealed that developing effective therapeutics against viruses might be outpaced by emerging variants, waning immunity, vaccine skepticism/hesitancy, lack of resources, and the time needed to develop virus-specific therapeutics, emphasizing the importance of non-pharmaceutical interventions as the first line of defense against virus outbreaks and pandemics. However, fighting the spread of airborne viruses has proven extremely challenging, much more if this needs to be achieved on a global scale and in an environmentally-friendly manner. Here, we introduce an aerosol filter media made of granular material based on whey protein nanofibrils and iron oxyhydroxides nanoparticles. The material is environmentally-friendly, biodegradable, and composed mainly of a dairy industry byproduct. It features filtration efficiencies between 95.91% and 99.99% for both enveloped and non-enveloped viruses, including SARS-CoV-2, the influenza A virus strain H1N1, enterovirus 71, bacteriophage Φ6, and bacteriophage MS2. While the filtration efficiencies were relatively high, they came at the cost of high pressure drop (≈0.03 bar). We believe that the methods and results presented here will contribute to advancing our understanding of granular-based aerosol filters, hopefully helping the design of highly-efficient granular media with low-pressure drops.

KEYWORDS

SARS-CoV-2, aerosol, filtration, amyloids, nanoparticles, environmentally friendly, protein-based materials, waste-valorization

1 Introduction

The development of vaccines and other therapeutics is an essential component of our panoply to fight viral pandemics. Therapeutics alone, however, might not be sufficient to end a pandemic at the desired speed, leading to potentially avoidable fatalities (Adam, 2022; Collaborators et al., 2022) and adverse socioeconomic consequences (Josephson et al., 2021). The emergence of new variants that can evade the immune response of vaccinated and convalescent patients (Pulliam et al., 1979; Liu et al., 2021; Colson et al., 2022; Mannar et al., 2022; Servellita et al., 2022), waning immunity (Evans et al., 2022; Thompson et al., 2022022; Gupta and Topol, 2021; Levine-tiefenbrun et al., 2022), vaccine skepticism/hesitancy (de Figueiredo and Larson, 2021; Kerr et al., 2021; Solís Arce et al., 2021), and lack of resources for production and administration of vaccines on a global scale within a short time period (Khamsi, 2020; Krammer, 2020; Liu et al., 2020; Forni et al., 2021; Sparrow et al., 2021; Wouters et al., 2021) are all factors that might compromise efforts to end a pandemic through therapeutics. Therefore, a key tool in this fight is preventing the transmission of viruses through non-pharmaceutical interventions (Hatchett et al., 2007; Flaxman et al., 2020; Perkins and España, 2020; Li et al., 2021; Morris et al., 2021). It has long been thought that the transmission of airborne viruses is mainly driven by droplets; (Wang et al., 1979; Samet et al., 2021); a growing body of evidence reveals that aerosols substantially contribute to airborne viral transmission, particularly in indoor spaces (Wang et al., 1979; Stadnytskyi et al., 2020; Samet et al., 2021; Lewis, 2022; Port et al., 2022). Mask mandates, social distancing, increased ventilation, and the use of air filters are measures used to combat airborne virus transmission in indoor spaces. Introducing air filters offers several advantages over other measures, i.e., they could contribute to maintaining indoor space capacities, offer a cost-effective solution for mechanically-ventilated spaces, and would be less sensitive to personal choices and/or behavioral discipline. High-efficiency particulate air (HEPA) filters constitute the gold standard for the filtration of aerosols. Producing HEPA filters requires relatively advanced fabrication technologies (Henning et al., 2021), with a large proportion made of either glass fibers or plastics, the former of which requires an energy-intensive fabrication process, and the latter of which relies heavily on the petrochemical industries (First, 1998; Henning et al., 2021). In addition, over time, a filter cake builds up on the fibers of the filter, resulting in increased resistance to airflow and the imminent need to replace the whole filter, with very limited options for cleaning and/or reuse (First, 1998). Indeed, using HEPA filters on a global scale to combat the transmission of airborne viruses in indoor spaces incurs prohibitive environmental and financial costs. Trying to combat a global pandemic using HEPA filters and other fiber-based filters is, in its essence, the outcome of being locked in a historical trap. Historically HEPA filters were developed to protect against airborne radioactive contaminants associated with the production of nuclear energy. For this purpose, it was necessary to achieve filtration efficiencies ≥99.97% of aerosols in the size range between 0.3 and 1.0 μm. None of these criteria is relevant to the filtration of airborne viruses, where the relevant efficiency is that of the reduction in the number of infectious viruses that go through the filter. Reduction in the number of infectious viruses can happen through trapping of the virus-containing aerosols and/or inactivation of the viruses during the filtration process. Different viruses are expected to have different inactivation efficiencies and are also likely to have different concentrations in aerosols with different sizes. Therefore, assessing the filtration efficiency based only on aerosol entrapment will likely result in an underestimation of the filtration efficiency for viruses, thus wrongly classifying filtration media as inadequate for virus filtration. This comes in crisis time, i.e., a pandemic, where such margins can make an immense difference in fighting the pandemic on a global scale.

In this work, we prepare a granular material composed of amyloid nanofibrils (AF) and iron (Fe) oxyhydroxides nanoparticles, i.e., AF-Fe. The material is environmentally friendly, biodegradable, and mainly composed of a diary industry byproduct (Palika et al., 2021). AF and Fe nanoparticles have been previously used as the building blocks of membrane filters for waterborne viruses, showing high efficiency in trapping viruses, including SARS-CoV-2, in bulk water (Palika et al., 2021). The rationale of this work was to use the same chemical building blocks as those used for the membrane filters to bring an additional advantage when filtering virus-loaded aerosols. Once the aerosols are trapped by the granular AF-Fe, the AF-Fe has the potential to inactivate and/or irreversibly attach the viruses in the trapped aerosols. The granular form of the material enables its application for aerosol filtration while increasing its mechanical stability, workability, and simplicity of handling. To assess the filtration efficiency of virus-loaded aerosols, we have designed and built a compact experimental setup that can be housed in laminar flow hoods of BSL2 and BSL3 laboratories. That setup was built to enable the direct assessment of the infectious viruses that pass through the filtration media. It complies with all biosafety regulations, enabling so far the first and only aerosol filtration study of SARS-CoV-2.

2 Results and discussion

2.1 Material fabrication and characterization

Using a facile fabrication process, we prepared a granular filtration material composed of amyloid nanofibrils and iron oxyhydroxides nanoparticles (AF-Fe), as shown in Figure 1A. The AF is prepared from whey protein extract, a by-product of the dairy industry, by lowering the pH to 2 and cooking at 90°C for ≈5 h. Afterward, Fe nanoparticles are precipitated on the fibrils by adding $FeCl_3{\cdot}6H_20$ and raising the pH to 7. A full characterization of the AF-Fe before converting it to the granular form has been reported earlier (Palika et al., 2021). The material is converted to a granular form by decanting the water from the material and baking it at 80°C-90°C. The material is then passed through a 12 US mesh sieve (pore size ≈1.7 mm) to remove larger pieces. However, larger aggregates of AF-Fe might form during packaging and storage (Figure 1B). The material, thus, has a broad size distribution with 50% of its mass smaller

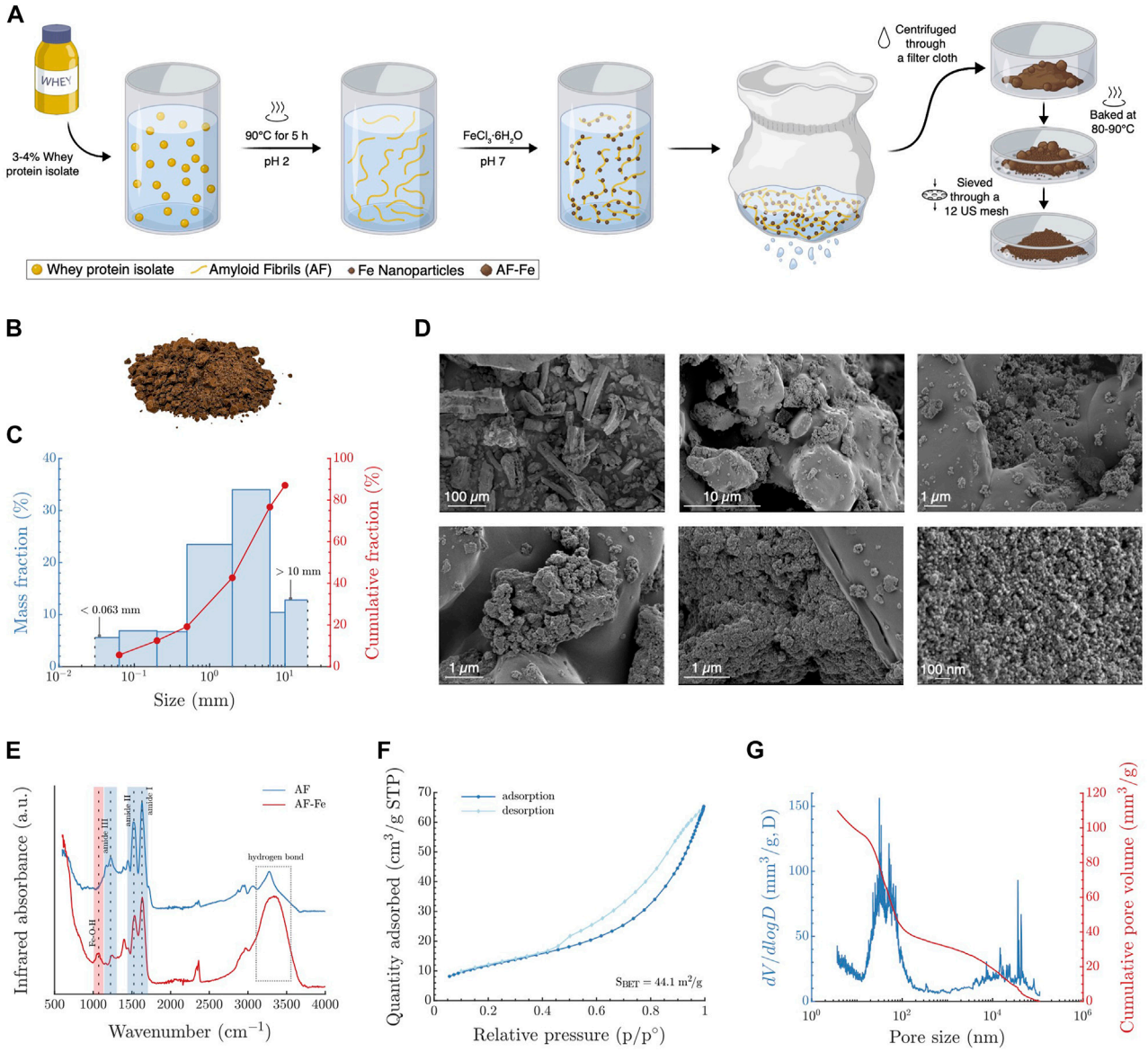

FIGURE 1
Fabrication and characterization of the granular AF-Fe. **(A)** A schematic showing the fabrication process of the AF-Fe. **(B)** A vectorized photo of the material after removing the background. **(C)** Size distribution of the AF-Fe determined using sieve analysis. **(D)** SEM micrographs of the material at varying magnifications. **(E)** FTIR analysis of both AF and AF-Fe. **(F)** N_2 adsorption analysis of the AF-Fe to determine its surface area. **(G)** Intra-particle pore size distribution of the AF-Fe determined using mercury intrusion porosimetry.

than 3 mm, as determined using sieve analysis (Figure 1C). Figure 1D shows scanning electron microscopy (SEM) micrographs of the material at various magnification scales where the iron oxyhydroxides nanoparticles can be visualized at the highest magnifications. The chemical composition of the material was further verified using Fourier transform infrared spectroscopy (FTIR; Figure 1E), which shows the three peaks for amide groups, representative of the amyloid fibrils, and one of the Fe-O-H group, representative of the iron oxyhydroxides nanoparticles. The material has a surface area of 44.1 $m^2\ g^{-1}$ (Figure 1F), i.e., the 50% surface coverage capacity of 1 g of the material is $\approx 7 \times 10^{14}$ and $\approx 3 \times 10^{13}$ for 30 or 150 nm virus particles, respectively. Its specific density, ρ_s, is 2.1 g cm^{-3} and bulk densities are 1.7 and 1.4 g cm^{-3} of air-equilibrated and oven-dried samples, respectively, showing a relatively high intra-particle porosity of 36% with 30% volumetric water content. The intra-particle pore-size distribution was further investigated using mercury intrusion porosimetry, revealing pores in size ranges of tens and thousands of nanometers (Figure 1G; Supplementary Figure S1). The size range of these pores has been previously suggested to serve as trapping cavities for viruses, preventing their release once they are attached to the surface of the AF-Fe (Canh et al., 2021). The material has a filling density of 0.99–1.04 g cm^{-3}, resulting in a relatively high inter-particle porosity of 39%–42%. Collectively, the properties of the granular AF-Fe make it a highly promising candidate for

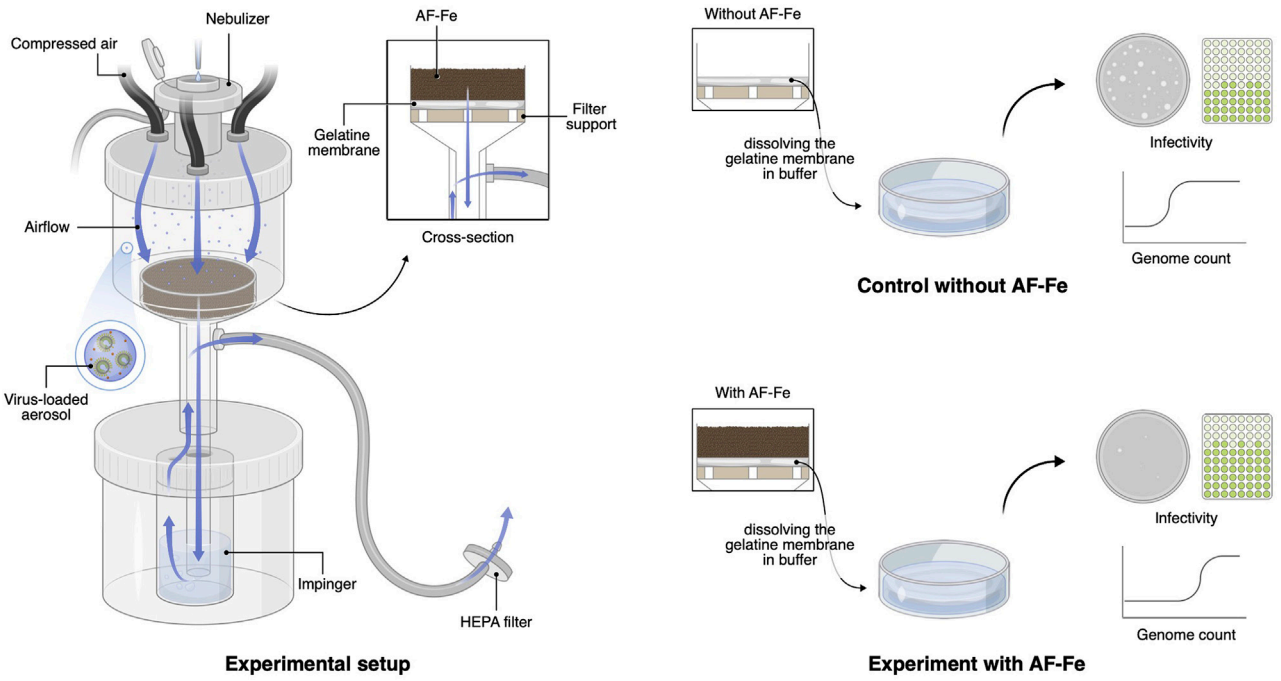

FIGURE 2
Schematic of the experimental setup and procedure. The experimental setup, left, is composed of: a filter holder with a nebulizer fitted on its top and three hoses connected to three compressed air tanks; the granular AF-Fe placed on a gelatine membrane, which traps the virus-loaded aerosols that pass through the AF-Fe media; an impinger serving as an additional trapping mechanism for any aerosols that go through the gelatine membrane; a HEPA filter as a third safety measure to avoid releasing any virus-loaded aerosols into the surrounding air. For both experiments with (bottom right) and without AF-Fe (top right), the gelatine membrane was dissolved in a buffer to determine the concentration of infectious viruses and the genome count.

filtering virus-loaded aerosols, with the potential of inactivating and/or irreversibly attaching viruses that come in contact with the material (Canh et al., 2021; Palika et al., 2021).

2.2 Experimental setup

To test the filtration efficiency of the material, we designed and built a compact experimental setup (Figure 2; Supplementary Figure S2) in which virus-loaded aerosols are generated, passed through the AF-Fe at a flowrate of 7.5 L min^{-1} (equivalent to face velocity of 7.2 cm s^{-1}), and then collected on a gelatine membrane that traps ≥99% of viruses passing through while maintaining their infectivity, as independently verified and detailed in Supplementary Figure S3. These gelatine membranes are water-soluble, facilitating virus extraction and subsequent infectivity and genome count assessment. The filtration efficiency of AF-Fe was determined by comparing the infectious viruses trapped on the gelatine membranes in the presence of AF-Fe versus in its absence. The setup is compact, allowing for complete operation inside of laminar flow hoods (Supplementary Figure S2). Additionally, all of its connections are tightly sealed, and its outlet tube is supplemented with an impinger and a HEPA vent (cytiva, Whatman, United Kingdom) to ensure safe operation, particularly when used to assess human viruses. To the best of our knowledge and by fulfilling all the biosafety requirements, this study is the first and so far only study that assesses the filtration of SARS-CoV-2-loaded aerosols. A detailed account of the setup, and the experimental procedure is presented in the Materials and Methods section.

2.3 Filtration efficiency of viruses

The filtration efficiencies of the AF-Fe against H1N1 (the influenza virus strain responsible for the flu pandemic in 2009) and SARS-CoV-2 were, on average, 99.87% and 95.91%, respectively (Figure 3A); both viruses are enveloped and known to be airborne. The filtration efficiency against the enterovirus EV71 was equal to 99.0% (Figure 3B); EV71 is non-enveloped, and is known for its stability and resistance to harsh chemical conditions. Due to safety concerns, most aerosol studies are conducted using bacteriophages (Turgeon et al., 2014). To situate our results in the context of the existing and future literature, we tested the efficiency of the AF-Fe against two of the most commonly used bacteriophages in aerosol studies: Φ6, an enveloped bacteriophage that infects *Pseudomonas syringae*; and MS2, a non-enveloped virus that infects *Escherichia coli*. The average filtration efficiency of Φ6 was found to be 99.99%, and that of MS2 98.29% (Figure 3C). The latter is known to be one of the most stable viruses in the aerosol phase and was previously estimated to be seven times more stable than coronaviruses (Turgeon et al., 2014). It is worth noting that the solution matrix was different for the different viruses (Methods Section for details), which might affect the size of the aerosols and, thus, the filtration efficiency.

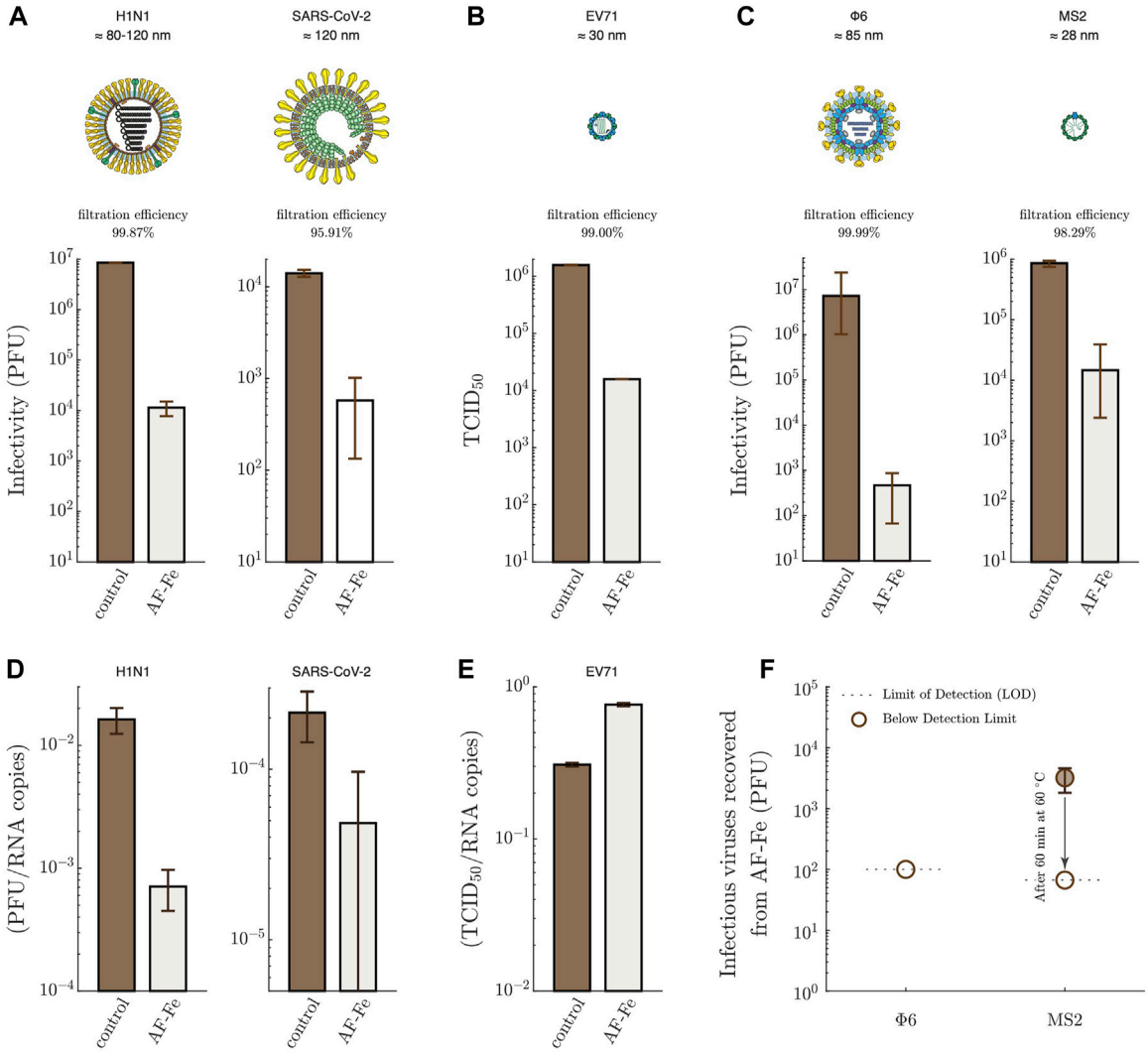

FIGURE 3
Filtration of virus-loaded aerosols using AF-Fe. Infectious viruses trapped on the gelatine membranes in the absence (control) and the presence of AF-Fe for H1N1 and SARS-CoV-2 **(A)**; EV71 **(B)**; Φ6 and MS2 **(C)**. The plotted values for H1N1 (control and AF-Fe), SARS-CoV-2 (control and AF-Fe), EV71 (control and AF-Fe), and Φ6 (AF-Fe) represent the average from two replicas, with the error bars representing the range. For Φ6 (control) and MS2 (control), the plotted values represent the average from four replicas, with the error bars representing the range. For MS2 (AF-Fe), the plotted value represents the average from three replicas, with the error bar representing the range. For H1N1, SARS-CoV-2, Φ6, and MS2, the infectivity was determined using plaque-forming units (PFU) assays. The infectivity of EV71 was determined using median tissue culture infectious dose ($TCID_{50}$). The ratio of infectious viruses to RNA copies, determined using RT-qPCR, is shown for H1N1 and SARS-CoV-2 **(D)**, and EV71 **(E)**. **(F)** Infectious viruses recovered after incubating the AF-Fe in PBS buffer for ≈1 h for both Φ6 and MS2. Representations of virions were reproduced with permission (Le Mercier, 2023)

Work on filtration of virus-loaded aerosols using granular material is very scarce, even less the work that involves human viruses. By screening the literature, we could identify only one recent and relevant study, which investigated the filtration of MS2-loaded aerosols using zero-valent nanosilver/titania-chitosan granules (Wang et al., 2021). When using the same thickness of the material we used, i.e., 2 cm, Wang et al. (2021) (Wang et al., 2021) achieved a filtration efficiency of ≈60%, compared to ≈98% for AF-Fe (Figure 3C). The higher filtration efficiency of AF-Fe is additionally complemented by the non-toxic nature of AF-Fe compared to the silver-based material. It is important to keep in mind that differences in the experimental conditions, such as the size distribution of aerosols, air flow rate, geometry of the filtration setup, and the capturing approach for the aerosol downstream of the filter, can also potentially affect the filtration efficiency across different studies. There are, however, more studies on the filtration of aerosols alone, i.e., virus-free aerosols, using granular media; some of these media reached an efficiency of 99.99% at face velocities comparable to our study, albeit using less sustainable materials and processes (Henning et al., 2021). These efficiencies are expected to be even higher if tested using virus-loaded aerosols due to the potential inactivation of viruses during the filtration process.

With no straightforward way to measure the pressure drop across the AF-Fe alone, i.e., without the filter support and the gelatin membrane, we opted for the approach detailed in the Supporting

Information in which the pressure in the upper chamber of the filtration setup was recorded using a digital manometer in the absence and presence of the AF-Fe. To put this in context with other filtration media, we also assessed the pressure drop across a HEPA membrane extracted from a HEPA vent (cytiva, Whatman, United Kingdom) using the same experimental approach. The results, as shown in Supplementary Figure S4, show that the pressure drop across the AF-Fe (≈0.03 bar) is close to that of the HEPA membrane (≈0.009 bar). We further tested the effect of reducing the amount of AF-Fe, and thus the pressure drop, on the filtration efficiencies. Using as low as two-thirds, 32 g, of the material, instead of 48 g, equivalent to a thickness of ≈2 cm, used in the reported experiments had little to no effect on filtration efficiencies (Supplementary Figures S5, S6) while reducing the pressure drop to two-thirds of its initial value (≈0.02 bar; Supplementary Figure S4). Therefore, the quality factor (QF) of the AF-Fe ranges between ≈0.001 and 0.005 Pa^{-1}, which is comparable to other granular-based materials but 1 to 2 orders of magnitude lower than fibrous and cellular media (Henning et al., 2021). Yet, these granular materials tend to come at a higher environmental footprint.

Figure 3D shows that the ratio of infectious H1N1 and SARS-CoV-2 to total genome count decreased after passing the AF-Fe, indicating that the viruses are not just trapped, but are also partially inactivated. A direct interaction between the viruses and AF-Fe would be needed for inactivation to occur. Part of the trapped aerosols is likely to be re-aerosolized again by the airflow shear forces. In this transient period of being attached to the AF-Fe, the viruses are inactivated. However, it also remains possible that the mechanical stress of re-aerosolization contributes to the observed inactivation. Such inactivation, however, was not observed for EV71 (Figure 3E), confirming that non-enveloped viruses are more robust and resistant to mechanical stresses due to the interactions with AF-Fe and the re-aerosolization process.

To assess the safe handling of the material, we incubated the AF-Fe for ≈1 h in phosphate-buffered saline (PBS) buffer after filtering aerosols loaded with Φ6 or MS2. No infectious viruses were recovered in the case of Φ6 (Figure 3F), indicating that the AF-Fe completely inactivated the virus and/or trapped it irreversibly. In the case of the non-enveloped MS2, < 0.5% of the infectious viruses were recovered, showing a remarkable capacity for irreversibly trapping the virus. Additionally, baking the AF-Fe at 60°C for 1 h was sufficient to completely inactivate MS2 to below the detection limit (Figure 3F). The baking temperature, 60°C, was chosen to be lower than the temperature used in the AF-Fe fabrication (80°C–90°C; Figure 1A) to avoid any damage or degradation of the AF-Fe. The inactivating and trapping capacity of AF-Fe is in agreement with previous work, where we showed that a membrane composed of AF and iron oxyhydroxides nanoparticles could eliminate viruses from bulk water to levels below the detection limit (Palika et al., 2021). For comparison, we have additionally tested the filtration efficiency of a HEPA membrane and the recovered infectious MS2 viruses from the membrane. While the HEPA efficiently trapped the virus-loaded aerosols to levels below the detection limit in the filtered air, it showed a lower inactivation/irreversible adsorption effect on MS2 compared to AF-Fe when >16 g of AF-Fe was used (Supplementary Figure S7). However, the significance of the antiviral properties of the filtration media while handling the material might be practically irrelevant because direct infection from contaminated filter media has not been previously reported in the literature, to the best of our knowledge.

2.4 Potential trapping mechanisms

The aerosol trapping mechanism of the AF-Fe is likely to have contributions from several sources, among which are the size, shape, roughness, charge, and hydrophobicity of the AF-Fe. Systematic experimental assessment of all these parameters is practically impossible, as there is no straightforward way to selectively vary one parameter while keeping the others constant. Despite its own limitations, which are discussed later, we restored to theoretical modeling to gain deeper insights into the contributions of the different aerosol trapping mechanisms. For this end, we modeled four key aerosol entrapment processes (Figure 4A): 1) diffusion, which is driven by Brownian motion of the aerosol droplets; 2) interception, which occurs when the airflow line comes within one aerosol radius distance from the grains of the filter; 3) gravitational settling, which is driven by gravitational forces acting on the aerosol particles; and 4) impaction, which is driven by the inertia of the aerosol particles. All of these processes depend on both the size of the AF-Fe grains, d_g, and the size of the aerosol droplets, d_a. Figure 4B (first four panels) shows that filtration efficiency due to diffusion decreases with increasing d_a; whereas, the efficiencies of interception, gravitational settling, and impaction increase with increasing d_a. The relative contributions of these mechanisms varied considerably with varying the size of grains. While these models were constructed for single-size grain filters, our AF-Fe filter has a very broad size distribution (Figure 1C, Supplementary Figure S8). To obtain more specific insights into our filter, we calculated an equivalent grain size, d_g = 0.139 mm, satisfying Ergun's equation (Equation S29) (Ergun, 1952), using the estimated pressure drop across the AF-Fe filter, 0.029 bar, as an input parameter (Figure 4B; last panel). Moreover, while the nominal size of aerosol produced by the nebulizer is 4–6 μm, we observed that many aerosols were between 0.1–1.0 μm in diameter at relative humidity, RH, between 80%–85% (Supplementary Figure S9). We, therefore, consider the whole aerosol size range between 0.1–10 μm in our discussion. Figure 4B; Supplementary Figure S10 suggest that diffusion and interception are the two key mechanisms for trapping aerosols ≲2 μm. For aerosol ≳2 μm, all three mechanisms, i.e., interception, gravitational settling, and impaction, exhibit very high efficiencies. The filtration efficiency curve presented in Figure 4B (last panel) resembles that of fiber-based filters, with diffusion, interception, and impaction being considered the key filtration mechanisms (First, 1998). Our results suggest that aerodynamic entrapment mechanisms (i.e., impaction, interception, diffusion, and gravitational settling), which depend only on the grain size, account for a substantial fraction of the observed filtration efficiency. Still, it is apparent from Figure 4 that the filtration efficiency predicted by the model is lower than the

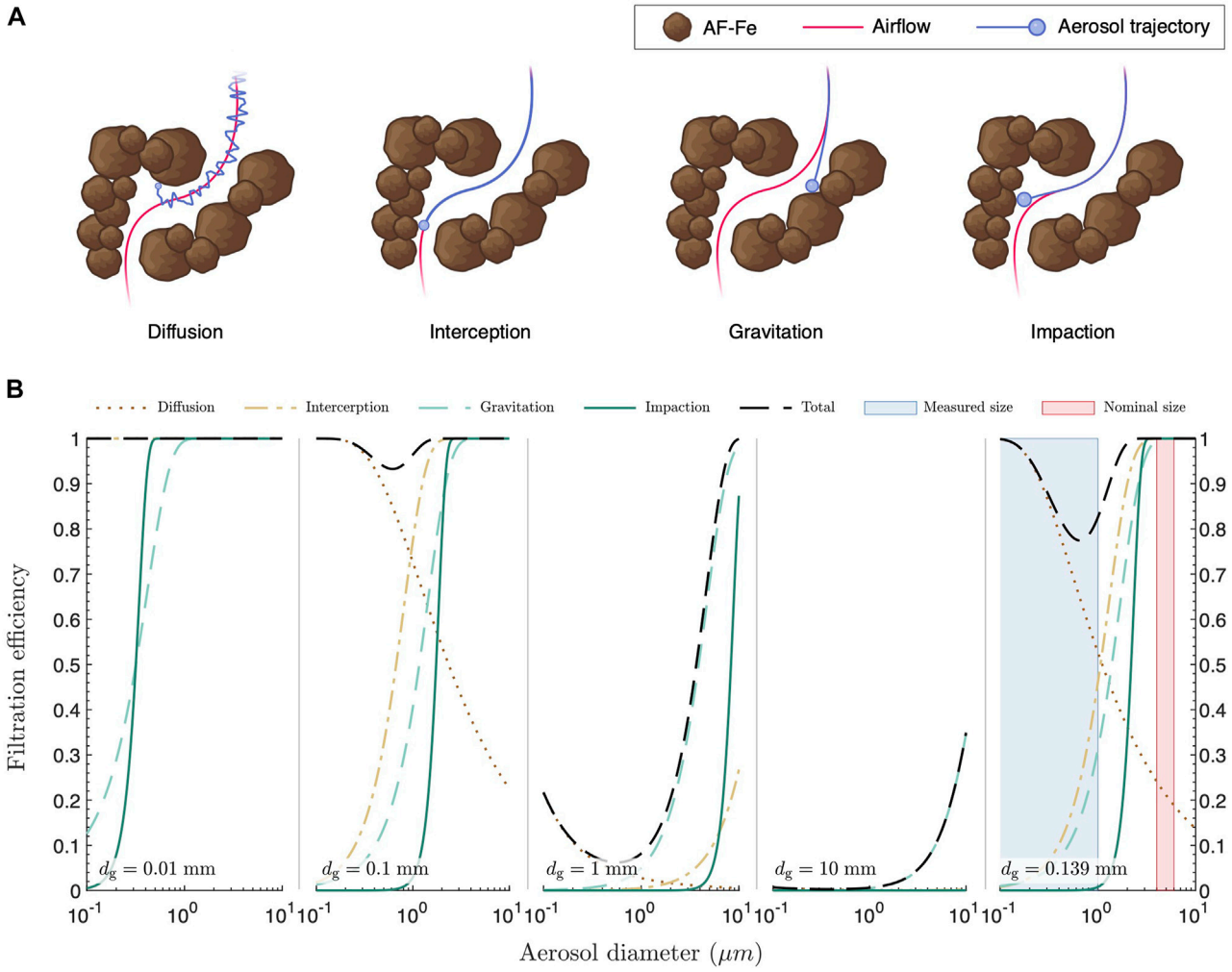

FIGURE 4
Mechanisms of aerosol entrapment. **(A)** Schematics depicting different processes involved in aerosol entrapment. **(B)** Filtration efficiencies due to diffusion, interception, gravitational settling, and impaction through grain bed filters with monodispersed grain size, d_g, which was varied systematically between 0.01 and 10 mm. d_g = 0.139 mm was calculated using Ergun's equation based on the measured pressure drop across the AF-Fe filter. In **(B)**, the nominal size indicates the diameter range of freshly nebulized droplets according to the manufacturer, while the measured size indicates the range of aerosol diameters at a relative humidity (RH) of 80%–85% (Supplementary Figure S9).

efficiencies as observed in Figure 3. These results suggest that other factors could make up for the remaining filtration efficiency of AF-Fe, namely polydispersity, irregular grain shape, roughness, charge, and/or hydrophilicity. However, drawing solid conclusions based on the model is not possible at the moment due to its several limitations. Future work on developing intricate models that consider the effect of these parameters would be necessary to obtain a more detailed and quantitative assessment of the mechanisms of aerosol filtration using grain-based filters, thus allowing the optimization of the grain properties to achieve even higher filtration efficiencies while reducing the pressure drop.

3 Conclusion

Altogether, our results demonstrate that AF-Fe can filter virus-loaded aerosols with very good efficiencies. There is, however, a need for substantial improvement in the pressure drop across the AF-Fe for the material to be comparable to existing filtration media and achieve economic and commercial feasibility. We foresee further developments in the design of granular-based material for aerosol filtration applications to simultaneously achieve high efficiencies and low pressure drops, while benefiting from the several advantages offered by granular material: e.g., broad availability in nature, ease of fabrication, safety of handling, and various options of recycling and reuse. The use of granular material for aerosol filtration in this study is also expected to inspire the search for new, local, environmentally-friendly materials that could also be used as the main building block for aerosol filters. Such research activities will be facilitated by the experimental setup used in this work, which fulfills all the biosafety requirements for studying emerging viruses in the aerosol phase while using affordable and easily accessible components.

4 Materials and methods

A full detailed version of the materials and methods is provided in the Supplementary Information. A summary of the most relevant sections is presented here.

4.1 Materials

AF-Fe. The granular AF-Fe material was provided by BluAct (Switzerland) and prepared as detailed later.

Viruses. SARS-CoV-2 virus hCoV-19/Switzerland/un-2012212272/2020 was a generous gift from Prof. Isabella Eckerle (University Hospital in Geneva, Geneva, Switzerland). The virus was replicated twice in Vero-E6 cells prior to the experiments. Human H1N1 virus A/Netherlands/602/2009 was a generous gift from Prof. Mirco Schmolke (Department of Microbiology and Molecular Medicine, University of Geneva, Geneva, Switzerland) and was propagated in embryonated chicken eggs (Riegger et al., 2015). Enterovirus 71 (EV71) was isolated from a clinical specimen in the University Hospital of Geneva in RD cells and propagated in Vero cells (Tseligka et al., 2018). Φ6 (21518 DSMZ) and MS2 (13767 DSMZ) bacteriophages were purchased from DSMZ culture collection (Germany) and propagated in their host bacterial cells.

4.2 Methods

Preparation of the AF-Fe granular material. Amyloid fibrils were prepared from whey protein isolate (BiPro, Agropur, United States) by lowering the pH to 2.0 and heating at 90°C for 5 h (Jung et al., 2008). Then, the amyloid fibrils were coated with iron nanoparticles by mixing $FeCl_3{\cdot}6H_2O$ and adjusting the pH to 7.0 using NaOH (Palika et al., 2021). The solution was then centrifuged through a filter cloth to decant the water. Afterward, the retentate was dried at 80°C-90°C and sieved through a 12 US mesh (pore size of ≈1700 μm) to remove large particles. It is important to note that some of the material formed larger aggregates during storage and packaging. The material is patented and produced by BluAct (Switzerland) and used as received without further treatment.

Assessment of aerosol filtration. The filtration efficiency of AF-Fe against virus-loaded aerosols was assessed using a compact experimental setup composed mainly of a polycarbonate filtration holder (Sartorius, Germany) connected to three 1.5 L compressed air tanks (PanGas, Switzerland) and an Aeroneb® Lab nebulizer unit (Kent Scientific, U.S.A.). Virus-containing solutions were prepared and added to the nebulizer: MS2 and Φ6 were prepared in artificial saliva/mucin solution, H1N1 in allantoid fluid, SARS-CoV-2 in high glucose Dulbecco's Modified Eagle Medium (DMEM, GlutaMAX™) supplemented with 2.5% fetal bovine serum (FBS), and EV71 in 2.5% serum DMEM. For each virus, 100 μL of the virus-containing solution was nebulized, generating aerosols with an average diameter of 4–6 μm, as indicated by the manufacturer, in the upper compartment of the filter holder. The generated aerosols were carried through the filtration media with the airflow from the compressed air tanks at 7.5 L/min (3 × 2.5 L/min). The aerosols passing through the AF-Fe media were then trapped using gelatine membranes (Sartorius, Germany). The membranes are water-soluble and designed to trap virus-loaded aerosols while retaining their infectivity. After disassembling the setup, the membranes were dissolved in 10 ml of PBS buffer for downstream analysis of infectivity and genome count of viruses. The efficiency of the AF-Fe media for the filtration of each virus was determined by comparing the infective viruses in the gelatine membrane in the presence versus the absence of the AF-Fe media. All experiments were conducted in a laminar flow hood.

Additional methods. Experimental details on the propagation of Φ6, MS2, H1N1, SARS-CoV-2, and EV71 viruses, infectivity assays, and RT-qPCR assays are given in full in the Supporting Information along with details on the materials and solutions used, experimental setup, and procedure for aerosol filtration, determination of AF-Fe size distribution, FTIR, SEM, N_2 adsorption, mercury intrusion porosimetry, water content and density determination, pressure drop measurements, determination of aerosol size distribution, and modeling aerosol entrapment mechanisms.

Data availability statement

The raw data supporting the conclusions of this article will be made available by the authors, without undue reservation.

Author contributions

AA designed the experimental setup for aerosol experiments; conducted all the aerosol experiments with Φ6, MS2, H1N1, and EV71; compiled the figures; and wrote the manuscript. HW (under the supervision of FS) conducted the aerosol experiments with SARS-CoV-2 and evaluated its infectivity. PA (under the supervision of MA) conducted the aerodynamics modeling and calculations; and performed the aerosol size distribution measurements. CM and AC-AZ (under the supervision of CT) propagated H1N1 and EV71, and evaluated their infectivity and genome count; evaluated the genome count of SARS-CoV-2. MP performed the FTIR and N2 adsorption experiments and analyzed their data. CG propagated Φ6 and MS2, and evaluated their infectivity for all aerosol experiments. SH carried out the SEM imaging. SB developed, synthesized, and provided the AF-Fe material. AA and RM wrote the manuscript. RM designed and directed the study; acquired funds; analyzed data; and wrote the manuscript. All authors edited and approved the final manuscript.

Funding

The authors gratefully acknowledge funding from the Swiss National Science Foundation project N° 31CA30_196217. Open access funding provided by ETH Zurich.

Acknowledgments

Martin Loessner (ETH Zurich) is deeply acknowledged for allowing access to his laboratory facilities; Isabella Eckerle, Manel

Essaidi-Laziosi, and Meriem Bekliz (University Hospital of Geneva, Switzerland) for providing SARS-CoV-2 strains; Daniel Kiechl, Peter Bigler, Carmen Saez Garcia Wanzenried, and Rasha Aziz (ETH Zurich) for providing excellent technical support; Michael Plötze from the ClayLab (ETH Zurich) for conducting the size distribution, density, and porosity determination experiments; Terttaliisa Lind (PSI) for valuable discussions; Sonia Monti for the design of scientific illustrations; Eleonora Simeoni, Vivianne Padrun, and Anna Maria Novello (EPF Lausanne) for biosafety support with SARS-CoV-2 experiments. The authors also gratefully acknowledge the support of the Scientific Center for Optical and Electron Microscopy (ScopeM) of the ETH Zurich.

Conflict of interest

RM and SB are the inventors of a filed patent application related to the work presented here. SB is employed by BluAct Technologies GmbH, Zurich, Switzerland. BluAct Technologies kindly donated the antiviral granular material studied in this work. All other authors declare that the research was conducted in the absence of any commercial or financial relationships that could be construed as a potential conflict of interest.

Publisher's note

All claims expressed in this article are solely those of the authors and do not necessarily represent those of their affiliated organizations, or those of the publisher, the editors and the reviewers. Any product that may be evaluated in this article, or claim that may be made by its manufacturer, is not guaranteed or endorsed by the publisher.

Supplementary material

The Supplementary Material for this article can be found online at: https://www.frontiersin.org/articles/10.3389/frsfm.2023.1143958/full#supplementary-material

References

Adam, D. (2022). 15 million people have died in the pandemic, WHO says. *Nature* 605, 206. doi:10.1038/d41586-022-01245-6

Canh, V. D., Tabata, S., Yamanoi, S., Onaka, Y., Yokoi, T., Furumai, H., et al. (2021). Evaluation of porous carbon adsorbents made from rice husks for virus removal in water. *Water (Basel)* 13 (9), 1280. doi:10.3390/w13091280

Collaborators, C.-19 E. M., Paulson, K. R., Pease, S. A., Watson, S., Comfort, H., Zheng, P., et al. (2022). Estimating excess mortality due to the COVID-19 pandemic: A systematic analysis of COVID-19-related mortality, 2020 – 21. *Lancet* 6736 (21), 1513–1536. doi:10.1016/S0140-6736(21)02796-3

Colson, P., Fournier, P.-E., Delerce, J., Million, M., Bedotto, M., Houhamdi, L., et al. (2022). Culture and identification of a "Deltamicron" SARS-CoV-2 in a three cases cluster in southern France. *J. Med. Virol.* 94, 3739–3749. No. March. doi:10.1002/jmv.27789

de Figueiredo, A., and Larson, H. J. (2021). Exploratory study of the global intent to accept COVID-19 vaccinations. *Commun. Med.* 1 (1), 30–10. doi:10.1038/s43856-021-00027-x

Ergun, S. (1952). Fluid flow through packed columns. *Chem. Eng. Prog.* 48 (2), 89–94.

Evans, J. P., Med, S. T., Evans, J. P., Zeng, C., Carlin, C., Lozanski, G., et al. (2022). Neutralizing antibody responses elicited by SARS-CoV-2 MRNA vaccination wane over time and are boosted by breakthrough infection. *Sci. Transl. Med.* 14, eabn8057. doi:10.1126/scitranslmed.abn8057

First, M. W. (1998). Hepa filters. *J. Am. Biol. Saf. Assoc.* 3 (1), 33–42. doi:10.1177/109135059800300111

Flaxman, S., Mishra, S., Gandy, A., Unwin, H. J. T., Mellan, T. A., Coupland, H., et al. (2020). Estimating the effects of non-pharmaceutical interventions on COVID-19 in europe. *Nature* 584, 257–261. doi:10.1038/s41586-020-2405-7

Forni, G., Mantovani, A., Forni, G., Mantovani, A., Moretta, L., Rappuoli, R., et al. (2021). COVID-19 vaccines: Where we stand and challenges ahead. *Cell Death Differ.* 28 (2), 626–639. doi:10.1038/s41418-020-00720-9

Gupta, R. K., and Topol, E. J. (2021). COVID-19 vaccine breakthrough infections. *Science* 374 (6575), 3741561–3741562. doi:10.1126/science.abl8487

Hatchett, R. J., Mecher, C. E., and Lipsitch, M. (2007). Public health interventions and epidemic intensity during the 1918 influenza pandemic. *Proc. Natl. Acad. Sci.* 104 (18), 7582–7587. doi:10.1073/pnas.0610941104

Henning, L. M., Abdullayev, A., Vakifahmetoglu, C., Simon, U., Bensalah, H., Gurlo, A., et al. (2021). Review on polymeric, inorganic, and composite materials for air filters: From processing to properties. *Adv. Energy Sustain. Res.* 2 (5), 2100005. doi:10.1002/aesr.202100005

Josephson, A., Kilic, T., and Michler, J. D. (2021). Socioeconomic impacts of COVID-19 in low-income countries. *Nat. Hum. Behav.* 5 (5), 557–565. doi:10.1038/s41562-021-01096-7

Jung, J. M., Savin, G., Pouzot, M., Schmitt, C., and Mezzenga, R. (2008). Structure of heat-induced β-lactoglobulin aggregates and their complexes with sodium-dodecyl sulfate. *Biomacromolecules* 9 (9), 2477–2486. doi:10.1021/bm800502j

Kerr, J. R., Schneider, C. R., Recchia, G., Dryhurst, S., Sahlin, U., Dufouil, C., et al. (2021). Correlates of intended COVID-19 vaccine acceptance across time and countries: Results from a series of cross-sectional surveys. *BMJ Open* 11 (8), 0480255–e48111. doi:10.1136/bmjopen-2020-048025

Khamsi, R. (2020). Can the world make enough coronavirus vaccine? *Nature* 580 (7805), 578–580. doi:10.1038/d41586-020-01063-8

Krammer, F. (2020). SARS-CoV-2 vaccines in development. *Nature* 586 (7830), 516–527. doi:10.1038/s41586-020-2798-3

Le Mercier, P. (2023). *ViralZone. SIB Swiss Institute of bioinformatics*.

Levine-tiefenbrun, M., Yelin, I., Alapi, H., Herzel, E., Kuint, J., Chodick, G., et al. (2022). Waning of SARS-CoV-2 booster viral-load reduction effectiveness. *Nat. Commun.* 13 (1237), 1237–1244. doi:10.1038/s41467-022-28936-y

Lewis, D. (2022). Why the WHO took two years to say COVID is airborne. *Nature* 604 (7904), 26–31. doi:10.1038/d41586-022-00925-7

Li, Y., Campbell, H., Kulkarni, D., Harpur, A., Nundy, M., Wang, X., et al. (2021). The temporal association of introducing and lifting non-pharmaceutical interventions with the time-varying reproduction number (R) of SARS-CoV-2: A modelling study across 131 countries. *Lancet Infect. Dis.* 21 (2), 193–202. doi:10.1016/S1473-3099(20)30785-4

Liu, L., Iketani, S., Guo, Y., Chan, J. F.-W., Wang, M., Liu, L., et al. (2021). Striking antibody evasion manifested by the omicron variant of SARS-CoV-2. *Nature* 602, 676–681. doi:10.1038/s41586-021-04388-0

Liu, Y., Salwi, S., and Drolet, B. C. (2020). Multivalue ethical framework for fair global allocation of a COVID-19 vaccine. *J. Med. Ethics* 46 (8), 499–501. doi:10.1136/medethics-2020-106516

Mannar, D., Saville, J. W., Zhu, X., Srivastava, S. S., Berezuk, A. M., Tuttle, K. S., et al. (2022). SARS-CoV-2 omicron variant: Antibody evasion and cryo-EM structure of spike protein–ACE2 complex. *Science* 375 (6582), 760–764. doi:10.1126/science.abn7760

Morris, D. H., Rossine, F. W., Plotkin, J. B., and Levin, S. A. (2021). Optimal, near-optimal, and robust epidemic control. *Commun. Phys.* 4 (78), 78–8. doi:10.1038/s42005-021-00570-y

Palika, A., Armanious, A., Rahimi, A., Medaglia, C., Gasbarri, M., Handschin, S., et al. (2021). An antiviral trap made of protein nanofibrils and iron oxyhydroxide nanoparticles. *Nat. Nanotechnol.* 16 (8), 918–925. doi:10.1038/s41565-021-00920-5

Perkins, T. A., and España, G. (2020). Optimal control of the COVID-19 pandemic with non-pharmaceutical interventions. *Bull. Math. Biol.* 82 (118), 118–124. doi:10.1007/s11538-020-00795-y

Port, J. R., Yinda, C. K., Avanzato, V. A., Schulz, J. E., Holbrook, M. G., van Doremalen, N., et al. (2022). Increased small particle aerosol transmission of B.1.1.7 compared with SARS-CoV-2 lineage A *in vivo*. *Nat. Microbiol.* 7 (2), 213–223. doi:10.1038/s41564-021-01047-y

Pulliam, J. R. C., van Schalkwyk, C., Govender, N., von Gottberg, A., Cohen, C., Groome, M. J., et al. (1979). Increased risk of SARS-CoV-2 reinfection associated with emergence of omicron in south Africa. *Science* 2022, 4947. doi:10.1126/science.abn4947

Riegger, D., Hai, R., Dornfeld, D., Mänz, B., Leyva-Grado, V., Sánchez-Aparicio, M. T., et al. (2015). The nucleoprotein of newly emerged H7N9 influenza A virus harbors a unique motif conferring resistance to antiviral human MxA. *J. Virol.* 89 (4), 2241–2252. doi:10.1128/jvi.02406-14

Samet, J. M., Burke, T. A., Lakdawala, S. S., Lowe, J. J., Marr, L. C., Prather, K. A., et al. (2021). SARS-CoV-2 indoor air transmission is a threat that can Be addressed with science. *Proc. Natl. Acad. Sci.* 118 (45), 21161551188–e2116155125. doi:10.1073/pnas.2116155118

Servellita, V., Morris, M. K., Sotomayor-Gonzalez, A., Gliwa, A. S., Torres, E., Brazer, N., et al. (2022). Predominance of antibody-resistant SARS-CoV-2 variants in vaccine breakthrough cases from the san francisco bay area, California. *Nat. Microbiol.* 7 (2), 277–288. doi:10.1038/s41564-021-01041-4

Solís Arce, J. S., Warren, S. S., Meriggi, N. F., Scacco, A., McMurry, N., Voors, M., et al. (2021). COVID-19 vaccine acceptance and hesitancy in low- and middle-income countries. *Nat. Med.* 27 (8), 1385–1394. doi:10.1038/s41591-021-01454-y

Sparrow, E., Wood, J. G., Chadwick, C., Newall, A. T., Torvaldsen, S., Moen, A., et al. (2021). Global production capacity of seasonal and pandemic influenza vaccines in. *Vaccine* 39 (3), 512–520. doi:10.1016/j.vaccine.2020.12.018

Stadnytskyi, V., Bax, C. E., Bax, A., and Anfinrud, P. (2020). The airborne lifetime of small speech droplets and their potential importance in SARS-CoV-2 transmission. *Proc. Natl. Acad. Sci. U. S. A.* 117 (22), 11875–11877. doi:10.1073/pnas.2006874117

Thompson, M. G., Natarajan, K., Irving, S. A., and Rowley, E. A. (2022). Effectiveness of a third dose of MRNA vaccines against COVID-19 – associated emergency department and urgent care encounters and hospitalizations among adults during periods of delta and omicron variant predominance — VISION network, 10 States. *Morb. Mortal. Wkly. Rep.* 71, 255–263.

Tseligka, E. D., Sobo, K., Stoppini, L., Cagno, V., Abdul, F., Piuz, I., et al. (2018). A VP1 mutation acquired during an enterovirus 71 disseminated infection confers heparan sulfate binding ability and modulates *ex vivo* tropism. *PLoS Pathog.* 14 (8), 10071900–e1007225. doi:10.1371/journal.ppat.1007190

Turgeon, N., Toulouse, M. J., Martel, B., Moineau, S., and Duchaine, C. (2014). Comparison of five bacteriophages as models for viral aerosol studies. *Appl. Environ. Microbiol.* 80 (14), 4242–4250. doi:10.1128/AEM.00767-14

Wang, C. C., Prather, K. A., Sznitman, J., Jimenez, J. L., Lakdawala, S. S., Tufekci, Z., et al. (1979). Airborne transmission of respiratory viruses. *Science* 2021 (6558), 373. doi:10.1126/science.abd9149

Wang, I. J., Chen, Y. C., Su, C., Tsai, M. H., Shen, W. T., Bai, C. H., et al. (2021). Effectiveness of the nanosilver/TiO2-chitosan antiviral filter on the removal of viral aerosols. *J. Aerosol Med. Pulm. Drug Deliv.* 34 (5), 293–302. doi:10.1089/jamp.2020.1607

Wouters, O. J., Shadlen, K. C., Salcher-Konrad, M., Pollard, A. J., Larson, H. J., Teerawattananon, Y., et al. (2021). Challenges in ensuring global access to COVID-19 vaccines: Production, affordability, allocation, and deployment. *Lancet* 397 (10278), 1023–1034. doi:10.1016/S0140-6736(21)00306-8